

# Super-Tonks-Girardeau quench of dipolar bosons in a one-dimensional optical lattice

Paolo Molignini<sup>1</sup> and Barnali Chakrabarti<sup>2</sup>

<sup>1</sup>*Department of Physics, Stockholm University, AlbaNova University Center, 10691 Stockholm, Sweden*

<sup>2</sup>*Department of Physics, Presidency University, 86/1 College Street, Kolkata 700073, India*

(Dated: January 22, 2024)

A super-Tonks-Girardeau gas is a highly excited yet stable quantum state of strongly attractive bosons confined to one dimension. This state can be obtained by quenching the interparticle interactions from the ground state of a strongly repulsive Tonks-Girardeau gas to the strongly attractive regime. While the super-Tonks-Girardeau quench with contact interactions has been thoroughly studied, less is known about the stability of such a procedure when long-range interactions come into play. This is a particularly important question in light of recent advances in controlling ultracold atoms with dipole-dipole interactions. In this study, we thus simulate a super-Tonks-Girardeau quench on dipolar bosons in a one-dimensional optical lattice and investigate their dynamics for many different initial states and fillings. By calculating particle density, correlations, entropy measures, and natural occupations, we establish the regimes of stability as a function of dipolar interaction strength. For an initial unit-filled Mott state, stability is retained at weak dipolar interactions. For cluster states and doubly-filled Mott states, instead, dipolar interactions eventually lead to complete evaporation of the initial state and thermalization consistent with predictions from random matrix theory. Remarkably, though, dipolar interactions can be tuned to achieve longer-lived prethermal states before the eventual thermalization. Our study highlights the potential of long-range interactions to explore new mechanisms to steer and stabilize excited quantum states of matter.

## I. INTRODUCTION

Rapid experimental advances in controlling ultracold atoms and their interactions are making it possible to realize and study enticing states of matter that encapsulate the exotic properties of quantum mechanics. These range from equilibrium phases such as supersolids and dipolar supersolids [1–14], to dynamical phenomena such as time crystals [15–17] and various Floquet phases [18–24]. Among these numerous recent advances, the super-Tonks-Girardeau (sTG) gas deserves special attention. The sTG is a quantum state of strongly attractive bosons confined to a one-dimensional (1D) geometry [25–29], and it is remarkable because it is stable despite being a highly excited state of matter. The sTG gas can be obtained from the standard Tonks-Girardeau (TG) gas [30–38] under sudden switching of contact interactions from the strongly repulsive to the strongly attractive regime. A possible explanation for the stability of the final state after the sudden quench relies on the sTG inheriting hardcore behavior from the TG gas [39] and the quenching process not causing any violent dynamics [40]. Besides providing a novel paradigmatic behavior, the realization of the sTG phase opens up the possibility of creating other quantum states of ultracold quantum gases with similar counter-intuitive properties [41, 42].

In particular, in recent experiments with 1D arrays of bosons, the stability of the sTG phase has been revisited by adding a weak dipole-dipole interactions (DDIs) between the atoms. In the experiment of Kao *et. al.* [29], the robustness of the sTG phase against collapse has been studied for a bosonic one-dimensional quantum gas of dysprosium atoms. Unexpectedly, even though the DDIs break the integrability, they enhance the stability of the sTG phase in comparison to the short-range interaction

case. This observation raises the prospect of employing weak dipolar forces to influence stability without changing the energy of the sTG phase significantly. This issue has been addressed recently by solving exactly a system of three trapped atoms with both contact and dipolar interactions [43], for which a distinct spectral response consisting of weaker hybridization with excited bound states is observed when repulsive DDIs are present. Another recent work [44] explores instead the unconventional mechanism of liquid formation in 1D optical lattice with strong on-site repulsion and weak long-range interactions. The underlying mechanism for liquid formation is established by a superexchange process. This discovery further prompted the investigation of the sTG quench in the corresponding geometry by means of extended Bose-Hubbard models, exploring the disruption of the states within a specific range of interactions [45].

Our work aims to describe a similar sTG quench in an optical lattice but with richer initial setups spanning more diverse states and particle fillings. This allows us to unravel intriguing physics in the quench dynamics. We mainly focus on a) clean Mott states and cluster states with unit filling and b) fermionized Mott states and cluster states with double filling. For each case, the strong short-range on-site repulsion is supplemented by four (for unit filling) and three (for double filling) specific cases of long-range dipolar interactions which correspond to different scenarios in the dynamical process. We present numerically exact many-body dynamics by solving the time-dependent many-boson Schrödinger equation utilizing the MultiConfigurational Time-Dependent Hartree method for bosons (MCTDHB) [46–52], implemented in the MCTDH-X software [53, 54]. We extract key measures such as one- and two-body density dynamics, natural occupations, many-body information entropy

and Glauber correlation functions. Our many-body dynamics highlights microscopic mechanisms not explored in earlier studies and provide understanding of the pathway from TG to sTG transition.

Besides highlighting new pathways to stable excited states of matter, studies on DDIs in STG states – such as the experiment by Kao *et. al* [29] – also give rise to strongly correlated prethermal states. In fact, prethermalization has emerged over the past decade as a ubiquitous phenomenon in the dynamics of ultracold quantum gases in 1D geometries [55–60]. Prethermalization happens when a many-body quantum system exhibits non-monotonic non-equilibrium dynamics: before reaching the true relaxed state (e.g. a thermal state), the system first relaxes to a short lived prethermal state which exhibits well separated intermediate time scales manifested by different values of certain observables, first among all in entropic quantities. This is contrast to the monotonic way of relaxation exhibiting a single time scale. While investigating the relaxation process in our STG quench dynamics, we encounter a highly nontrivial time evolution that leads to prethermalization. In particular, we show how to control the long-range interactions to create a long-lived prethermal states or short-lived quasi-prethermal states.

Our overall observations are as follows: While the TG gas without dipolar perturbation is stable under the sTG quench, all weakly bound and scattering Mott states and all cluster states collapse and lose all correlations – a process termed *evaporation*. The evaporation occurs at different time scales depending on the strength of the DDIs and we can trace clear many-body features before it actualizes. Furthermore, the fermionized Mott state exhibits even more intriguing expansion dynamics before evaporation. In terms of entropy dynamics, perfect thermalization is observed both for the clean Mott states and deep self-bound cluster states. However, for very weak attractive long-range interactions, some quasi-stationary states at intermediate time scales emerge. This establishes how long-range interactions can be taken as a control parameter to create prethermal or quasi-prethermal states with longer lifetimes.

The rest of this paper is structured as follows. In section II, we expostulate the theory behind the system we investigate and the quenching protocols we implement in our simulations. In section III, we briefly review the main features of our methods and we define the observables used to track the post-quench dynamics. In sections IV and V we present our results for respectively unit and double filling and discuss their significance. Finally, in section VI, we summarize the main findings of our paper and give an outlook on potential future research directions.

## II. SYSTEM AND PROTOCOL

We are interested in the dynamics of a system of  $N$  interacting bosons of mass  $m$  in a one-dimensional lattice, which is governed by the time-dependent many-body Schrödinger equation

$$\hat{H}\psi = i\hbar\frac{\partial\psi}{\partial t}. \quad (1)$$

The total Hamiltonian has the form

$$\hat{H}(x_1, x_2, \dots, x_N) = \sum_{i=1}^N \hat{h}(x_i) + \sum_{i<j=1}^N \hat{W}(x_i - x_j). \quad (2)$$

Its one-body part is  $\hat{h}(x) = \hat{T}(x) + \hat{V}_{OL}(x)$ , where  $\hat{T}(x) = -\frac{\hbar^2}{2m}\frac{\partial^2}{\partial x^2}$  is the kinetic energy operator and  $\hat{V}_{OL}(x) = V_0 \sin^2(k_0 x)$  is the external 1D lattice of depth  $V_0$  and wave vector  $k_0$ . Unless otherwise stated, we will keep  $V_0$  fixed at  $20 E_r$ , where  $E_r = \frac{\hbar k_0}{2m}$  is the recoil energy of the lattice. This depth is necessary to reach the Mott regime in the state preparation. We restrict the geometry to encompass  $S$  sites in the optical lattice (defined as the spatial extent between two maxima in the sinusoidal function) adding hard-wall boundary conditions at each end. The two-body interactions  $\hat{W}(x_i - x_j)$  contain both short-range  $W_C(x_i, x_j) = g_0 \delta(x_i - x_j)$  and long-range dipolar interactions  $W_D(x_i, x_j) = \frac{g_d}{|x_i - x_j|^{3+\alpha}}$ . Here,  $g_0$  is the strength of the local interactions, which is strongly positive before the quench and suddenly becomes negative after the quench,  $g_d$  controls the strength of the long-range interactions and it is negative all throughout our calculations, and  $\alpha$  denotes a renormalization factor used to avoid nonphysical singularities at  $x_i = x_j$ . Without long-range interactions, the ground state of the system is either in the TG phase (with one particle per site) or the fermionized TG phase (with more than one particle per site). With strong negative DDIs, the ground state is a cluster state at one site in the optical lattice and possesses distinguished many-body features. Weakly negative DDIs interpolate between these two cases. We remark that the Hamiltonian  $\hat{H}$  can be written in dimensionless units obtained by dividing the dimensionful Hamiltonian by  $\frac{\hbar^2}{mL^2}$ , with  $L$  an arbitrary length scale, which for the sake of our calculations we will set to be the period of the optical lattice.

With this Hamiltonian, we will study two different setups. First, we consider a unit filling scenario of  $N = 5$  particles in  $S = 5$  sites. Then, we explore a more correlated double filling setup, with  $N = 6$  particles in  $S = 3$  sites. The protocol in both cases is identical. We first obtain the ground state for the Hamiltonian with strong contact repulsion ( $g_0^{t<0} \gg 0$ ). Then, at time  $t = 0$ , we propagate this state by quenching it to the strongly attractive regime of equal magnitude ( $g_0^{t\geq 0} \ll 0$ ,  $|g_0^{t\geq 0}| = g_0^{t<0}$ ). In the experiments, this is achieved by exploiting a confinement-induced resonance (CIR), where

particle interactions are enhanced in a confined space such as a trap or potential well [33, 34, 61–66]. By means of Feshbach resonance techniques, it is possible to control the  $s$ -wave contact interaction and effectively control the long-range interaction. We study the stability of the sTG state during the time evolution for different values of the attractive dipolar interactions  $g_d$ . Our additional motivation is to find the time scale of relaxation and possibly confirm the existence of any prethermal states.

### III. METHODS

To investigate the dynamics of dipolar bosons under the sudden quench, we employ the MultiConfigurational Time-Dependent Hartree method for indistinguishable particles (MCTDHB) [46–49] implemented by the MCTDH-X software [49–54]. MCTDH-X solves the many-body Schrödinger equation by recasting the many-body wave function as an adaptive superposition of  $M$  time-dependent single-particle wave functions, called orbitals. Both the coefficients and the basis functions in this superposition are optimized in time to yield either ground-state information (via imaginary time propagation) or full-time dynamics (via real-time propagation). We refer to the Appendix A for further details on this method. In our calculations, we employ  $M = 10$  orbitals for the unit filling case of  $N = 5$  particles in  $S = 5$  sites, and  $M = 12$  orbitals for the double filling case of  $N = 6$  particles in  $S = 3$  sites. Our choice of number of orbitals thus guarantees an average of at least two orbitals per site in each case and the required convergence is assured.

To extract information from the system, we calculate several observables. To probe the spatial distribution of the bosons, we calculate the one-body density from the many-body state  $|\Psi(t)\rangle$  as

$$\rho(x; t) = \langle \Psi(t) | \hat{\Psi}^\dagger(x) \hat{\Psi}(x) | \Psi(t) \rangle. \quad (3)$$

To measure the degree of coherence and many-body correlation, we calculate the reduced one-body and two-body densities, defined respectively as

$$\rho^{(1)}(x, x'; t) = \langle \Psi(t) | \hat{\Psi}^\dagger(x) \hat{\Psi}(x') | \Psi(t) \rangle \quad (4)$$

$$\rho^{(2)}(x, x'; t) = \langle \Psi(t) | \hat{\Psi}^\dagger(x) \hat{\Psi}^\dagger(x') \hat{\Psi}(x') \hat{\Psi}(x) | \Psi(t) \rangle. \quad (5)$$

To study statistical relaxation and thermalization in the quench dynamics, the information theoretical measure known as Shannon information entropy is the ideal quantity [67, 68]. We define here an equivalent measure of information entropy called occupation entropy. This is based on the assumption that in MCTDHB with time evolution the many-body state can exhibit dynamical fragmentation, i.e. several natural orbitals exhibit significant population. We thus define the occupation information entropy as

$$S_{\vec{n}}(t) = - \sum_{\vec{n}, i} \frac{n_i(t)}{N} \ln \left( \frac{n_i(t)}{N} \right), \quad (6)$$

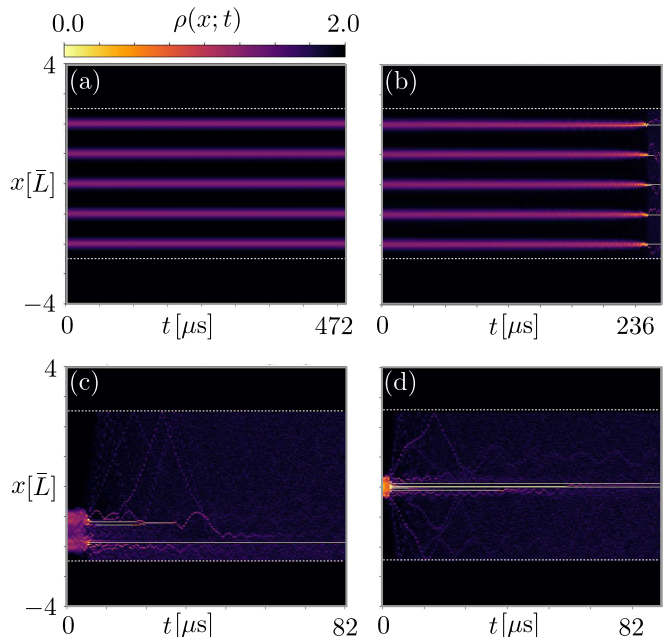


FIG. 1. Density dynamics post quench for  $N = 5$  bosons and  $M = 10$  orbitals in  $S = 5$  sites (unit filling) with (a)  $g_d = 0.0E_r$ , (b)  $g_d = -0.45E_r$ , (c)  $g_d = -0.82E_r$ , (d)  $g_d = -2.02E_r$ . The other parameters are  $V_0 \approx 20E_r$  and  $|g_0| \approx 81E_r$ . The dotted lines indicate the system boundaries.

where  $n_i(t)$  is the occupation of the  $i$ -th element of the many-body configuration  $\vec{n}$  (see appendix A for details). In the Gross-Pitaevskii single orbital mean-field theory, as the reduced density matrix has a single eigenvalue,  $S_{\vec{n}}$  is zero. For multiconfigurational states, instead, when several configurations contribute to the many-body state,  $S_{\vec{n}} \neq 0$ . As more and more orbitals start to populate the many-body state,  $S_{\vec{n}}(t)$  gradually increases and finally saturates to a value determined by the maximally fragmented many body state.

### IV. RESULTS FOR UNIT FILLING

We begin our analysis by presenting the results for the unit filling case of  $N=5$  bosons in  $S = 5$  sites. In this section, unless otherwise stated, the magnitude of the contact interactions is fixed at  $|g_0| \approx 81E_r$ . We have probed a fine array of dipolar interactions in the range  $g_d \in [-3.6E_r, 0E_r]$ , but we will only show representative results to be concise.

#### A. Evaporation mechanism

The density dynamics is plotted in Fig. 1(a)-(d) for four representative values of  $g_d$  showcasing the appearance of different dynamical behaviors. Fig. 1(a) demonstrates the TG to sTG quench for  $g_d = 0$ . In this scenario, the pre-quench state is a fully fragmented clean

Mott state in the TG limit (see appendix C for an overview of the initial states), which has positive energy and remains highly stable for very long time after the quench. Upon turning on the dipolar attractions, for  $g_d = -0.45E_r$ , the bosons initially retain their Mott structure. However, the post-quench stability is reduced and the particles eventually evaporate as shown in Fig. 1(b). When the long-range attractions are increased further, e.g. to  $g_d = -0.82E_r$ , the bosons progressively deviate from the Mott state and form clusters pinned around a subset of the total number of lattice sites. The system still has positive energy, but due to the effect of long-range interactions all the five bosons are confined within a subset of five lattice sites. Upon quenching, the state first demonstrates very intriguing many-body expansion dynamics and subsequently evaporates as shown in Fig. 1(c). We remark that the time scale for this process is extremely short (evaporation begins already around  $10 \mu\text{s}$ ) compared to the time scale for the emergence of instability in the clean Mott state. For even stronger attractions, which correspond to the self bound Mott phase with negative energy, the bosons form a cluster state in the central lattice and upon quenching the evaporation is extremely fast – in the order of  $5 \mu\text{s}$ . This is illustrated in Fig. 1(d) for  $g_d = -2.02E_r$ . In both Fig. 1(c) and (d), the diverging nature of long-range interactions is clear: the density is propelled externally, hits the walls of the lattice, bounces back, and forms a distorted interference pattern.

To clearly explore the many-body features in the sTG quench, we present snapshots of the reduced one-body density  $\rho^{(1)}(x, x', t)$  and two-body density  $\rho^{(2)}(x, x', t)$  for some chosen times in Fig. 2 and Fig. 3, respectively. For the TG state at  $g_d = 0.0E_r$ , the one-body density is perfectly diagonal, indicating only self-correlation within each Mott peak. The two-body density, exhibits a completely depleted region along the diagonal – termed “correlation hole” – which is a manifestation of fermion-like exclusion stemming from the strong repulsion that makes the bosons act as hard-core particles. As already seen from the density, the TG to sTG quench at zero dipolar interactions [Figs. 2(a)-(c) and 3(a)-(c)] is stable for very long times, and both the diagonal shape of  $\rho^{(1)}$  and the correlation hole of  $\rho^{(2)}$  persist at all probed times. However, when the dipolar interactions are increased such that an eventual instability appears [Figs. 2(d)-(f) and 3(d)-(f)], the diagonal (off-diagonal) pattern in  $\rho^{(1)}$  ( $\rho^{(2)}$ ) is maintained only until a critical time, which for the chosen point at  $g_d = -0.45E_r$  is approximately  $260 \mu\text{s}$ . After that, a rather sudden collapse and eventual evaporation of all correlations occur. Further increasing the interactions, e.g. to  $g_d = -0.82E_r$ , leads to a phase transition from the TG Mott state to a progressively more localized cluster state, which is apparent also in the correlation functions [Figs. 2(g)-(i) and 3(g)-(i)]. Five bright spots in  $\rho^{(1)}$  distinguish the existence of five strongly interacting bosons at  $t = 0$ . After the quench, at a very small time ( $t = 5.94 \mu\text{s}$ ), the central atom loses its iden-

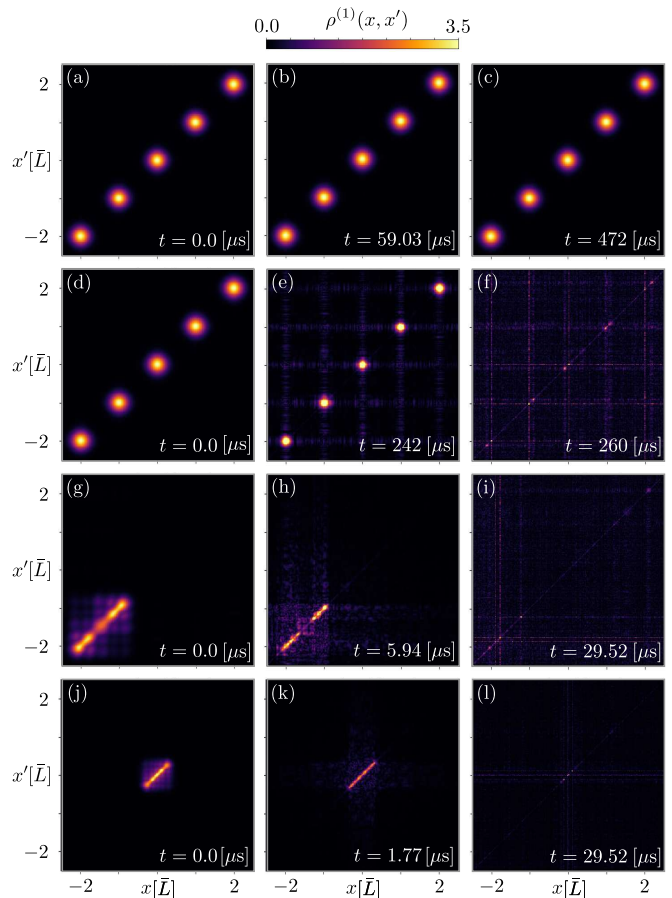


FIG. 2. Dynamics of the reduced one-body density  $\rho^{(1)}(x, x')$  post quench for  $N = 5$  bosons and  $M = 10$  orbitals in  $S = 5$  sites (unit filling) with (a)-(c)  $g_d = 0.0E_r$ , (d)-(f)  $g_d = -0.45E_r$  (g)-(i)  $g_d = -0.82E_r$ , (j)-(l)  $g_d = -2.02E_r$ . The other parameters are  $V_0 \approx 20E_r$  and  $|g_0| \approx 81E_r$ .

tity, whereas two atoms on each side of it retain their identity although a bit diminished. At  $t = 29.52 \mu\text{s}$ , we observe complete disruption. However, four very faded traces are visible across the diagonal. Interestingly, the two-body density exhibits correlation across the entire system, even though the density seems localized on the left-hand side. Upon quenching, it spreads and becomes uniform across the whole diagonal and gradually evaporates. For  $g_d = -2.02E_r$ , deep in the cluster state, five bright central spots in  $\rho^{(1)}$  and a central correlation region in  $\rho^{(2)}$  again configure the existence of five bosons. After the quench, they follow the same evaporation process but in a much faster time scale. We remark that the evaporation process is not “macroscopic”; not all the five bosons evaporate simultaneously. It is rather microscopic; the outermost bosons evaporate first and are followed by the rest of the central atoms.



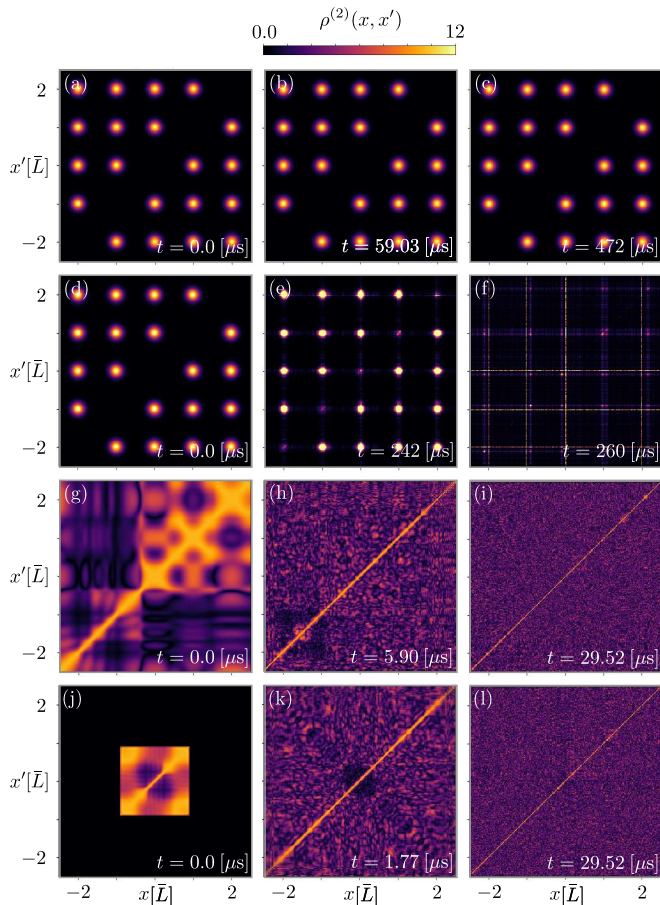


FIG. 3. Dynamics of the reduced two-body density  $\rho^{(2)}(x, x')$  post quench for  $N = 5$  bosons and  $M = 10$  orbitals in  $S = 5$  sites (unit filling) with (a)-(c)  $g_d = 0.0E_r$ , (d)-(f)  $g_d = -0.45E_r$  (g)-(i)  $g_d = -0.82E_r$ , (j)-(l)  $g_d = -2.02E_r$ . The other parameters are  $V_0 \approx 20E_r$  and  $|g_0| \approx 81E_r$ .

### B. Emergence of statistical relaxation and prethermalization

The onset of thermalization in an isolated quantum system with a finite number of interacting particles is an established issue in theoretical physics [69]. The necessary condition for thermalization is statistical relaxation, whereupon various observables settle to some kind of equilibrium. The emergence of prethermalization is characterized by the establishment of a quasi-stationary state at intermediate time scales, followed by relaxation to a stationary state at much longer time scales. Physical origin of prethermalization is still elusive and primarily supposed to be related to integrability modified by external perturbation or quasi-integrability. The time scale of prethermalization in complex many-body systems is crucially determined by the range of interaction and particle number [70]. In the present work, as the sTG phase demonstrates strong many-body correlation and its stability depends on the strength of weak dipolar interactions, we utilize the quenched state to understand the

relaxation process, its time scale and the possibility of induce prethermalization.

Many-body information entropy measures such as  $S_{\bar{n}}(t)$  defined by Eq. (6) are generally considered as the ideal quantities to study statistical relaxation [67, 68]. To investigate statistical relaxation of the post quench state, we then plot the time evolution of  $S_{\bar{n}}$  for different choices of long-range interactions in Fig. 4. As the entropy evolution is very closely related to the occupation in different orbitals and dynamical fragmentation, we also plot the dynamics of the natural occupations in Fig. 5.

For the TG gas without long-range interactions, whose ground state is a five-fold fragmented Mott state, the lowest five orbitals exhibit equal population each of  $1/N = 0.2$ . Throughout the dynamics, as shown in Fig. 5(a), there is no change in fragmentation because the state is stable against the quenching procedure. Thus, the occupation information entropy remains constant at the initial value of  $S_{\bar{n}} \approx 1.61$  as shown in Fig. 4(a).

Now, it is also interesting to assess this constant value utilizing the prediction from the Gaussian orthogonal ensemble (GOE) of random matrices [71]. For time reversal and rotationally invariant systems, statistical relaxation follows the prediction of GOE which estimates  $S_{\bar{n}}^{\text{GOE}} = -\sum_{i=1}^M \frac{1}{M} \ln \left[ \frac{1}{M} \right] = \ln M$ , where  $M$  is the significantly contributed number of orbitals exhibiting dynamical fragmentation. For the TG to sTG quench without long-range interactions the GOE prediction is then  $S_{\bar{n}}^{\text{GOE}} \approx 1.609$  as the system exhibits five-fold fragmentation throughout the dynamics; thus out of  $M = 10$  orbitals only  $M = 5$  orbitals are populated. As we can see from Fig. 4(a), the post-quench entropy dynamics perfectly saturates to the value of the GOE prediction.

For  $g_d = -0.45E_r$ , Fig. 5(b) shows that initially the system retains five-fold fragmentation as the long-range interaction is weakly attractive. Upon quenching, the system remains highly stable until time  $t \approx 236 \mu\text{s}$ , when suddenly the system breaks its stability and becomes fully fragmented. Thus, initially  $M = 5$  orbitals contribute in fragmentation as well as in the entropy measure, whereas upon complete fragmentation all the  $M = 10$  orbitals become equally populated. The corresponding entropy measure in Fig. 4(b), starts with the GOE predicted value  $\approx 1.61$  ( $M = 5$ ) and then increases and saturates at the GOE estimate with  $M = 10$  orbitals, i.e.  $S_{\bar{n}}^{\text{GOE}} \approx 2.30$ , which is concomitant with the complete relaxation process to an evaporated gas state.

For  $g_d = -0.82E_r$  and  $g_d = -2.02E_r$  the system becomes fully fragmented very fast as observed in Fig. 5 (c) and (d) respectively. The corresponding entropy production is shown Figs. 4 (c)-(d). In both cases, the entropy measure starts from the initial value close to the GOE prediction, then steeply increases and at the time of complete fragmentation it finally saturates perfectly to GOE estimate. The steep increase in the occupation entropy reflects an exponential increase in the number of excited states participating in the many-body dynamics.

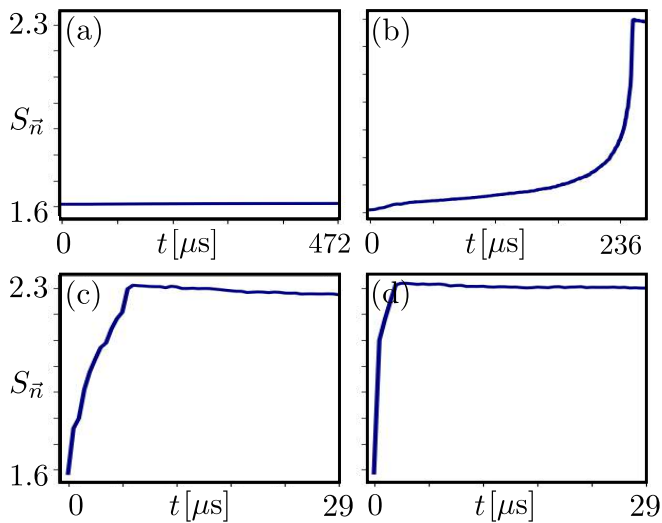


FIG. 4. Dynamics of occupation entropy for  $N = 5$  bosons and  $M = 10$  orbitals in  $S = 5$  sites (unit filling) with (a)  $g_d = 0.0E_r$ , (b)  $g_d = -0.45E_r$ , (c)  $g_d = -0.82E_r$ , (d)  $g_d = -2.02E_r$ . The other parameters are  $V_0 \approx 20E_r$  and  $|g_0| \approx 81E_r$ .

For both cases perfect relaxation is achieved and one single time scale is exhibited, although for larger attractive long-range interactions the relaxation happens very fast.

It is also interesting to examine whether the system with long-range attractive interactions always exhibits the monotonic nonequilibrium dynamics or it is possible that before reaching the true relaxed state, the system may exhibit one or several intermediate time scales and more complex relaxation dynamics. To investigate that, we reduce the lattice depth to  $V_0 \approx 8E_r$  and slowly control very weak attractive long-range interaction. Results are presented in Fig. 6 for few selected choices of  $g_d$ . It is clearly seen that initially all entropy measures start from  $\approx 1.61$  and eventually saturate to  $\approx 2.3$  at time  $t = 59 \mu s$ . However, they also exhibit intermediate plateaus, where an almost constant entropy is held for certain time. One can define a time  $\tau_{\text{pre}}$ , as the time for which the prethermal state survives. This is a well separated time scale from the eventual relaxation time scale. We find that  $\tau_{\text{pre}}$  is longer for weaker long-range attractions,  $g_d = -0.2E_r$  and  $-0.4E_r$ . With slow tuning and making the long-range interactions stronger, the lifetime of the prethermal state begins to decrease, it becomes quasi-prethermal and then disappears, finally exhibiting single timescale nonequilibrium dynamics for  $g_d \geq 1.0E_r$ . This phenomenology indicates that the long-range interaction strength can act as a controlling parameter to reveal relaxation processes in several steps, through well separated timescales. We also find that with other, suitable choices of lattice depths and quenching strengths it is possible to create similar intermediate prethermal or quasi-prethermal states.

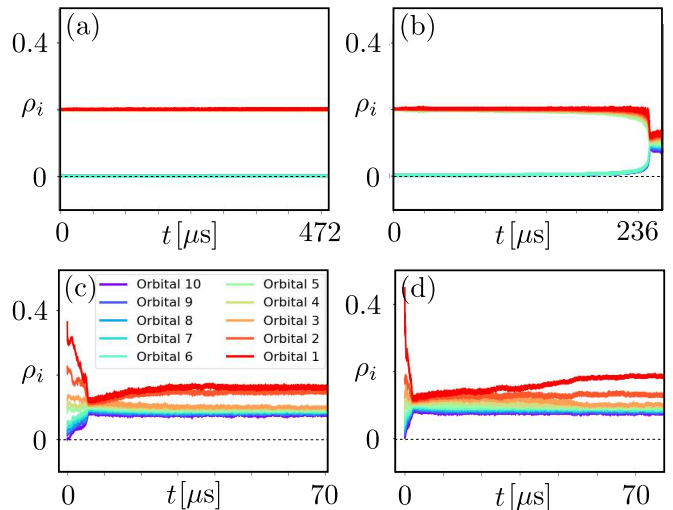


FIG. 5. Dynamics of orbital occupation for  $N = 5$  bosons and  $M = 10$  orbitals in 5 sites (unit filling) with (a)  $g_d = 0.0E_r$ , (b)  $g_d = -0.45E_r$ , (c)  $g_d = -0.82E_r$ , (d)  $g_d = -2.02E_r$ . The other parameters are  $V_0 \approx 20E_r$  and  $|g_0| \approx 81E_r$ .

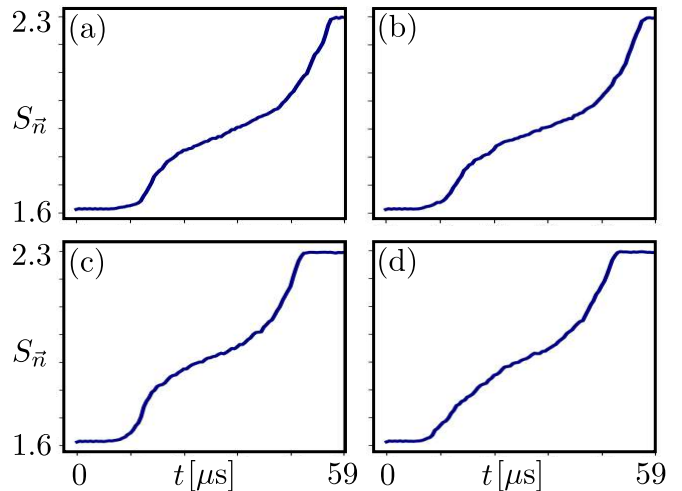


FIG. 6. Dynamics of occupation entropy for  $N = 5$  bosons and  $M = 10$  orbitals in  $S = 5$  sites (unit filling) with  $V_0 \approx 8E_r$ ,  $|g_0| = 20E_r$  and (a)  $g_d = -0.2E_r$ , (b)  $g_d = -0.4E_r$ , (c)  $g_d = -0.6E_r$ , (d)  $g_d = -0.8E_r$ .

## V. RESULTS FOR DOUBLE FILLING

We now present results for more exotic doubly-filled initial states consisting of  $N=6$  bosons in  $S = 3$  sites. Unless otherwise stated, we keep the magnitude of the contact interactions at  $|g_0| \approx 81E_r$  and probe the same range of dipolar interactions  $g_d \in [-3.6E_r, 0E_r]$  as in the single filling case, showing a handful of representative cases.

Fig. 7 illustrate the post-quench density dynamics for increasing values of DDIs  $g_d$ . For all the values of DDIs probed, we find that the system is very unstable to the sudden quench and the density rapidly evaporates. For

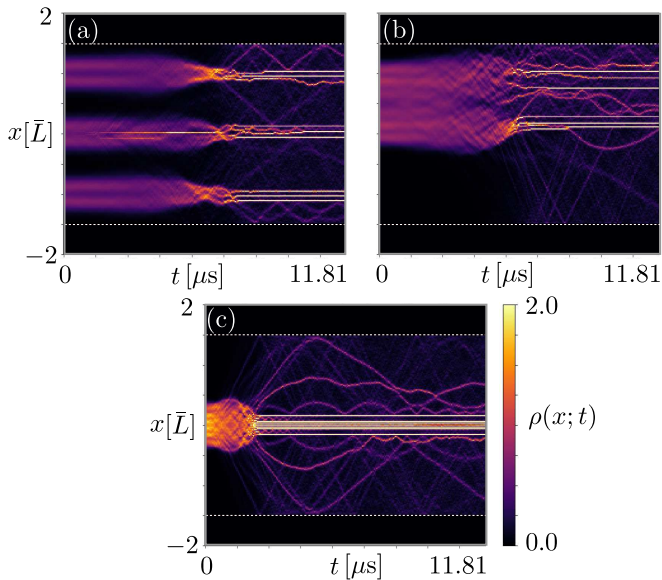


FIG. 7. Density dynamics post quench for  $N = 6$  bosons and  $M = 12$  orbitals in  $S = 3$  sites (double filling) with (a)  $g_d = 0.0E_r$ , (b)  $g_d = -0.82E_r$ , (c)  $g_d = -2.02E_r$ . The other parameters are  $V_0 \approx 20E_r$  and  $|g_0| \approx 81E_r$ . The dotted lines indicate the system boundaries.

$g_d = 0.0$ , the initial state consists of pairs of bosons located at the minima of the optical lattice (we again refer to appendix C for detail on the initial states). Because of the strong contact repulsion, the initial many-body wave function is already fragmented and the particles at each site are spatially separated in dimers—it is a fermionized Mott phase. Upon quenching, the configuration is stable only for short times of around  $6 \mu\text{s}$ , comparable to the stability of the unit-filling cluster states, after which evaporation and total fragmentation occur, see Fig. 7(a). This is in stark contrast to the unit filling case, where the TG state at  $g_d = 0.0$  exhibits extreme stability. We thus reveal that the stability of the STG state does not survive multiple filling. When the dipolar interactions are turned on, the initial state becomes more clustered. The cluster state is contended by two consecutive lattice sites while keeping the third one completely empty due to frustration emerging between lattice localization, attractive long range interactions and repulsive contact interactions. However, the cluster state clearly exhibits the presence of six bosons: in the density dynamics six bright jets propagate for short time before losing their stability (Fig. 7(b)). By further increasing the dipolar interactions, we achieve an initial cluster state tightly self-bound around the center of the optical lattice. However, six clear humps in the initial density exhibits six strongly correlated bosons in the fermionized limit. Similarly to the fate of the cluster state in the unit filling case, this state is very unstable to quenching. It survives for only a few  $\mu\text{s}$ , before evaporating by rapidly ejecting particles outward as shown in Fig. 7(c).

The mechanism for the evaporation process at differ-

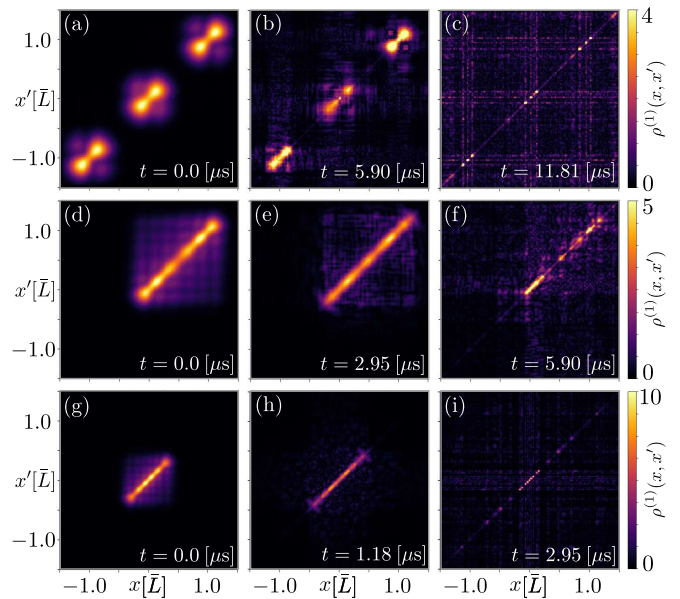


FIG. 8. Dynamics of the reduced one-body density  $\rho^{(1)}(x, x')$  post quench for  $N = 6$  bosons and  $M = 12$  orbitals in  $S = 3$  sites (double filling) with (a)-(c)  $g_d = 0.0E_r$ , (d)-(f)  $g_d = -0.82E_r$ , (g)-(i)  $g_d = -2.02E_r$ . The other parameters are  $V_0 \approx 20E_r$  and  $|g_0| \approx 81E_r$ .

ent dipolar interaction strengths becomes clearer upon examining the one-body and two-body reduced density matrices visualized in Figs. 8 and 9. For the dimerized initial states at both zero and non-zero  $g_d$ , the bosons clearly exhibit non-zero off-diagonal one-body correlation within each dimer already at time zero [Figs. 8(a),(d)]. This act as a channel that allows to dissipate correlation away from the main diagonal, leading to subsequent evaporation at later times [Figs. 8(b)-(c),(e)-(f)]. This cross-correlation between different particles is not present in the TG Mott state at unit filling. A similar mechanism is at play also for the cluster state achieved at stronger dipolar interactions [Figs. 8(g)], but in this case the evaporation occurs at even faster rate [Figs. 8(h)-(i)].

In the two-body reduced density matrix, the structure of the dimerized state is clearly visible both in the off-diagonal peaks and in the diagonal correlation hole [Figs. 9(a),(d)]. Upon quenching, the correlation hole is rapidly reduced while at the same time off-diagonal correlation evaporates. Note, however, that the initial geometric structure of the initial state is visible at later times after evaporation has taken place [Figs. 9(c),(f)]. For the cluster state, a similar initial structure is present, albeit with a much smaller correlation hole due to the self-confinement of the bosonic particles [Figs. 9(g)]. The sudden quench immediately destroys the correlation hole and induces correlation in the outward-ejected particles [Figs. 8(h)]. The process rapidly culminates into evaporation of the cluster state into very fragmented single-particle states.

Finally, we briefly examine the occupation and entropy



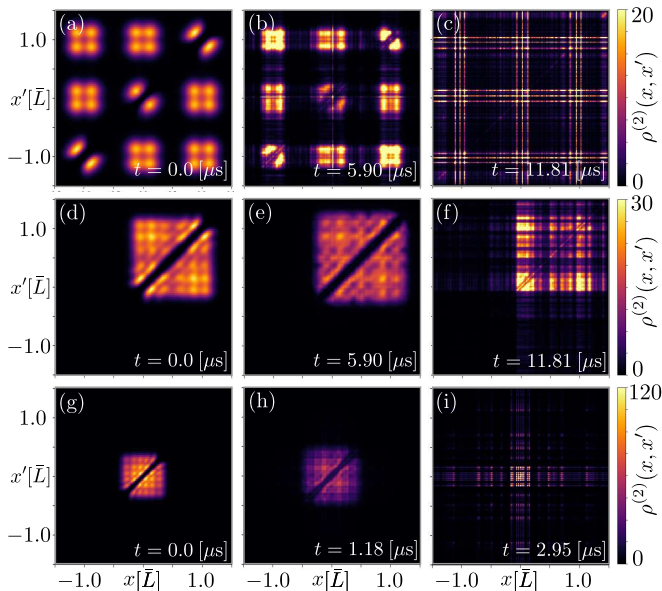


FIG. 9. Dynamics of the reduced two-body density  $\rho^{(2)}(x, x')$  post quench for  $N = 6$  bosons and  $M = 12$  orbitals in  $S = 3$  sites (double filling) with (a)-(c)  $g_d = 0.0E_r$ , (d)-(f)  $g_d = -0.82E_r$ , (g)-(i)  $g_d = -2.02E_r$ . The other parameters are  $V_0 \approx 20E_r$  and  $|g_0| \approx 81E_r$ .

behavior of the three representative double-filling states examined thus far. A plot of the occupation entropies is shown in Fig. 10 whereas the evolution of the natural occupations is depicted in Fig. 11. All doubly filled states become completely fragmented very fast – in the order of  $10 \mu s$  – and all the orbitals acquire the same population of  $1/12$ . The corresponding entropy measures in Fig. 10 (a)-(c), show saturation to GOE estimate  $S_{\vec{n}}^{\text{GOE}} \approx 2.48$  at longer time for all three choices of long-range interactions. For strong attractive long-range interactions with  $g_d = -2.02E_r$ , relaxation happens in a single timescale and possibility of prethermalization is ruled out. However, for weaker long-range interaction some additional features are exhibited in the entropy dynamics at intermediate timescale, which signifies the possibility for the existence of extremely short-lived quasi-prethermalization behavior before increasing almost linearly towards the GOE estimate.

## VI. CONCLUSIONS

We have investigated the quench dynamics of strongly-interacting bosons in an optical lattice for a wide range of dipolar interaction strengths and different fillings, generalizing the STG quench procedure to the presence of long-range interactions and more exotic initial states. Our protocol consisted in preparing an initial state of bosons with strong contact repulsions and dipolar attractions, and then quenching the strength of the contact interactions to the strongly negative (attractive) regime. We

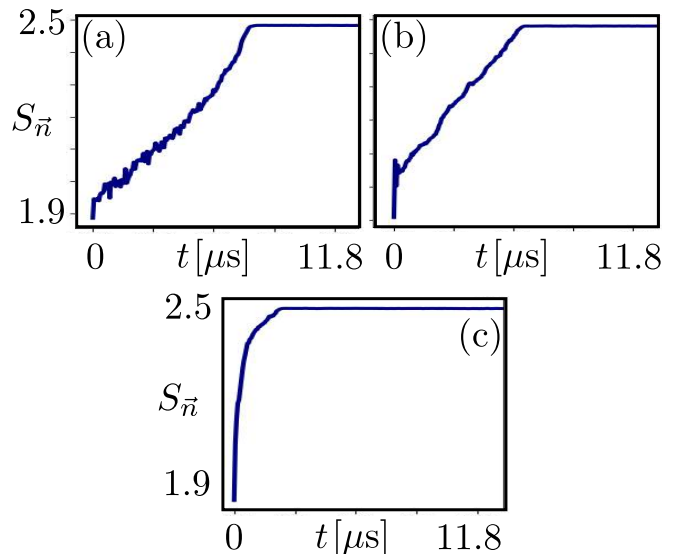


FIG. 10. Dynamics of occupation entropy for  $N = 6$  bosons and  $M = 12$  orbitals with (a)-(b)  $g_d = 0.0E_r$ , (c)-(d)  $g_d = -0.82E_r$ , (e)-(f)  $g_d = -2.02E_r$ . The other parameters are  $V_0 \approx 20E_r$  and  $|g_0| \approx 81E_r$ .

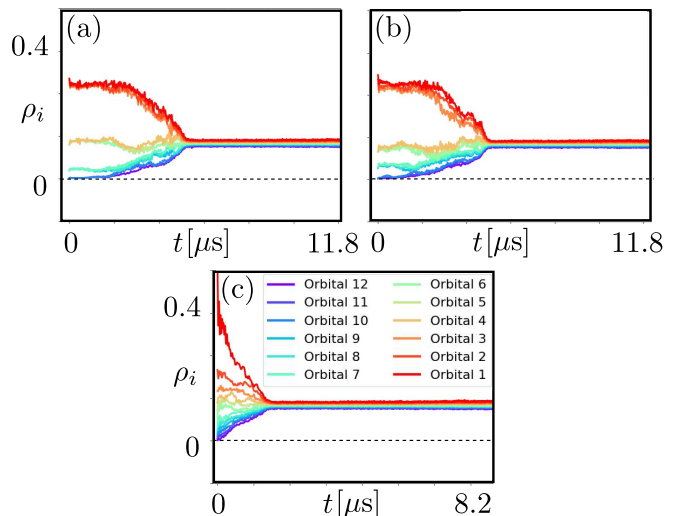


FIG. 11. Dynamics of orbital occupation for  $N = 6$  bosons and  $M = 12$  orbitals in three sites (double filling) with (a)  $g_d = 0.0E_r$ , (b)  $g_d = -0.82E_r$ , (c)  $g_d = -2.02E_r$ . The other parameters are  $V_0 \approx 20E_r$  and  $|g_0| \approx 81E_r$ .

have calculated numerous observables to study the time evolution, including one-body density, reduced one-body and two-body densities, entropy measures, and natural occupations. By analyzing these quantities, we have mapped out the effect of different dipolar interaction strengths on the stability of the post-quench states.

As expected, starting from a unit-filled Mott state at zero dipolar interactions we recollect the robustness of the original STG quench, where the localized Mott peaks remain unperturbed for a very long time. At weak dipolar interactions, this stability is retained only for a



shorter time. By increasing the dipolar interactions further, the initial bosonic configuration condenses into a cluster state. The cluster state is much more sensitive to the quench procedure and rapidly evaporates into a chaotic state well-described by a thermal Gaussian orthogonal ensemble that maximizes entropy measures. A similar fate is observed by starting from doubly filled states, be them in dimerized Mott configurations (low dipolar interactions) or cluster states (high dipolar interactions). The state rapidly evaporates ejecting particles with complex many-body dynamics that leads to complete fragmentation and thermalization. By examining measure of correlations, we find that the cause for this behavior lies within the structure of the initial states, that exhibit pockets of correlations within the dimers or within different peaks of the cluster states. These pockets of correlations spread upon quenching and lead to instability and eventual evaporation.

However, we have also established that the pathway towards thermalization can be drastically altered by tuning the magnitude of the interactions and of the optical lattice depth. It is possible to obtain prethermal states that survive for longer times before the eventual entropy saturation. Empirically, we find that this behavior is obtained using moderate dipolar interactions strengths in the order of up to one recoil energy. This finding is consistent with previous literature predictions for the appearance of prethermalization due to long-range interactions.

Our study sheds light onto the behavior and stability of strongly correlated bosonic states in the presence of long-ranged interactions. It also showcases the potential of harnessing such long-range interactions and quenching protocols to achieve novel pathways to the creation and control of excited quantum states of matter. These questions are particularly timely since the systems we have investigated should be easily engineered in state-of-the-art ultracold experiments, e.g. with magnetic quantum gases [72]. The complex atomic structure and the large dipole moment of these systems facilitate the control of the interatomic interaction strength, specially the relative strength of contact over dipolar interactions. This will lead to further exploration of few and many-body physics.

In the future, we envision that similar approaches could be employed to study the complex interplay of different energy scales introduced by the competition between localizing optical lattices, local (contact) interactions, and long-range interactions, which could lead to a multitude of exotic quantum states. Our study could also be extended to analyze the stability of other fermionization and crystallization phenomena, potentially in higher dimensions or fostered by other kind of long-range interactions, e.g. mediated by cavities [73, 74]. This last setup is particularly promising as it has been shown to give rise to a plethora of intriguing equilibrium and out-of-equilibrium phases of matter, such as higher-order superfluidity, Mott phases, and limit cycles [75–78]. It would be interesting to analyze whether the interplay of such

phases with dipolar interactions could lead to a stabilization of prethermal states. Another interesting route to pursue is the connection with the accuracy of dipolar quantum simulators [79]. Our method solves the many-body Schrödinger equation in the continuum, and thus should be an accurate representation of the physics at play in the actual quantum simulators and not just in the simulated lattice models (e.g. extended Bose-Hubbard models) studied elsewhere in the literature. For example, a relevant question to ask is to what extent a similar STG quench would lead the physics to deviate from that of a lattice model as a function of dipolar interaction strength, optical lattice depth, and other system parameters. It could also include the investigation of quantum many-body scar states which can give rise to infinitely long-lived coherent dynamics under quantum quenches from well controlled initial states [80]. Another open avenue for future studies is the impact of long-range interactions on quantum holonomy – where parameters are tuned to realized a cycle starting from the free system, to Tonks-Girardeau and super-Tonks-Girardeau regimes, and then back to the free system [81]. The comparison between sudden quench and adiabatic quench will help to understand the underlying correlation dynamics. Furthermore, continuous quenches will provide information on defect dynamics and criticality by means of Kibble-Zurek formalism [82, 83].

*Acknowledgements* – We thank Emil Bergholtz for useful discussions. This work was supported by the Swedish Research Council (2018-00313) and Knut and Alice Wallenberg Foundation (KAW) via the project Dynamic Quantum Matter (2019.0068). Computation time at the High-Performance Computing Center Stuttgart (HLRS) and on the Euler cluster at the High-Performance Computing Center of ETH Zurich is gratefully acknowledged.

## Appendix A: MCTDH-X

In this appendix, we briefly review the numerical method used to obtain the time evolution of the few-boson systems presented in the main text. We employ the MultiConfigurational Time-Dependent Hartree method for indistinguishable particles implemented by the MCTDH-X software [49–54].

MCTDH-X constructs the many-body wave function as a linear combination of time-dependent permanents

$$|\Psi(t)\rangle = \sum_{\mathbf{n}} C_{\mathbf{n}}(t) |\mathbf{n}; t\rangle. \quad (\text{A1})$$

The permanents are constructed over  $M$  time-dependent single-particle wavefunctions, called orbitals, as

$$|\mathbf{n}; t\rangle = \prod_{k=1}^M \left[ \frac{(\hat{b}_k^\dagger(t))^{n_k}}{\sqrt{n_k!}} \right] |0\rangle \quad (\text{A2})$$

Here,  $\mathbf{n} = (n_1, n_2, \dots, n_M)$  is the number of bosons in each orbital. This is constraint by  $\sum_{k=1}^M n_k = N$ , with

$N$  the total number of bosons. Allocating  $N$  bosons over  $M$  orbitals, the number of permanents becomes  $\binom{N+M-1}{N}$ . Additionally,  $|0\rangle$  is the vacuum state and  $\hat{b}_k^\dagger(t)$  denotes the time-dependent operator that creates one boson in the  $k$ -th working orbital  $\psi_k(x)$ , *i.e.*:

$$\hat{b}_k^\dagger(t) = \int dx \psi_k^*(x; t) \hat{\Psi}^\dagger(x; t) \quad (\text{A3})$$

$$\hat{\Psi}^\dagger(x; t) = \sum_{k=1}^M \hat{b}_k^\dagger(t) \psi_k(x; t). \quad (\text{A4})$$

The accuracy of the algorithm depends on the number of orbitals used. For  $M = 1$  (a single orbital), MCTDH-X coincides with a mean-field Gross-Pitaevskii description. For  $M \rightarrow \infty$ , the wave function becomes exact as the set  $|n_1, n_2, \dots, n_M\rangle$  spans the complete  $N$ -particle Hilbert space. For practical calculations, we restrict the number of orbitals to a value that is small enough to achieve convergence in the relevant observables.

Both the expansion coefficients  $C_{\mathbf{n}}(t)$  and the working orbitals  $\psi_i(x; t)$  that constitute the permanents are optimized variationally at every time step [84] to either relax the system to its ground state (imaginary time propagation), or to calculate the full dynamics of the many-body state (real time propagation). The variational procedure occurs at the level of the many-body action obtained from the Hamiltonian of the system written in second quantization as

$$\hat{\mathcal{H}} = \int dx \hat{\Psi}^\dagger(x) \left\{ \frac{p^2}{2m} + V(x) \right\} \hat{\Psi}(x) + \frac{1}{2} \int dx \hat{\Psi}^\dagger(x) \hat{\Psi}^\dagger(x') W(x, x') \hat{\Psi}(x) \hat{\Psi}(x'), \quad (\text{A5})$$

where  $V(x)$  denotes a one-body potential and  $W(x, x')$  describes two-body interactions. For the present work,  $V(x)$  is the optical lattice, while  $W(x, x')$  is the sum of contact repulsion and dipole-dipole interactions. We require the stationarity of the action with respect to variations of the time-dependent coefficients and orbitals. This results in a coupled set of equations of motion containing those quantities, which are then solved simultaneously. We remark that the one particle function  $\phi_i(x, t)$  and the coefficient  $C_{\bar{n}}(t)$  are variationally optimal with respect to all parameters of the many-body Hamiltonian at any time [84–87].

From the working orbitals, it is possible to calculate  $N$ -body reduced density matrices and obtain information about correlation in the system. For example, the one-body reduced density matrix can be computed as

$$\rho^{(1)}(x, x') = \sum_{kq=1}^M \rho_{kq} \psi_k(x) \psi_q(x'), \quad (\text{A6})$$

where

$$\rho_{kq} = \begin{cases} \sum_{\mathbf{n}} |C_{\mathbf{n}}|^2 n_k, & k = q \\ \sum_{\mathbf{n}} C_{\mathbf{n}}^* C_{\mathbf{n}^k} \sqrt{n_k(n_q + 1)}, & k \neq q \end{cases} \quad (\text{A7})$$

and the sum runs over all possible configurations of  $\mathbf{n}$ . The quantity  $\mathbf{n}_q^k$  denotes the configuration where one boson is extracted from orbital  $q$  and then added to orbital  $k$ . The one-particle density can be then easily computed from the one-body reduced density matrix as its diagonal elements:

$$\rho(x) = \rho^{(1)}(x, x)/N \quad (\text{A8})$$

## Appendix B: System parameters

In this appendix we discuss the parameters for the simulations presented in the main text. The system consists of  $N = 5$  or  $N = 6$  bosons in an optical lattice with lattice depth  $V_0$  and wave vector  $k_0 = \pi/\lambda$  parametrized as

$$V(x) = V_0 \sin^2(k_0 x). \quad (\text{B1})$$

We choose the wavelengths to be compatible with real experimental realizations in ultracold atomic labs, *i.e.*  $\lambda_0 \approx 532.2$  nm. This gives a wave vector  $k_0 \approx 5.903 \times 10^6$  m<sup>-1</sup>. Depending on the setup, we set hard-wall barriers to restrict the optical lattice to the center-most five minima (single-filling simulations) or three minima (double-filling simulations).

### 1. Lengths

In MCTDH-X simulations, we choose to set the unit of length  $\bar{L} \equiv \lambda_0/2 = 266.1$  nm, which makes the minima of the optical lattice (the sites in the lattice picture) appear at integer values in dimensionless units, while the maxima are located at half-integer values. In particular,  $x = 0$  acts as the center of the lattice which can host an odd number of sites  $S$ . In our simulations, we consider mainly two cases: an integer filling of  $N = 5$  bosons in  $S = 5$  sites, and a double filling of  $N = 6$  bosons in  $S = 3$  sites. In both cases, we run simulations with 512 gridpoints in an interval  $x \in [-4\bar{L}, 4\bar{L}] \approx [-1.064\mu\text{m}, 1.064\mu\text{m}]$ , giving a resolution of around 4.158 nm. We employ hard-wall boundary conditions at  $x = \pm 2.5$  ( $S = 5$ ) and  $\pm 1.5$  ( $S = 3$ ) to clearly demarcate the end of the optical lattice.

### 2. Energies

The unit of energy  $\bar{E}$  is effectively defined in terms of the recoil energy of the optical lattice, *i.e.*  $E_r \equiv \frac{\hbar^2 k_0^2}{2m} \approx 2.204 \times 10^{-30}$  J with  $m \approx 51.941$  Da the mass of <sup>52</sup>Cr atoms, a dipolar species amply used in experiments [88, 89]. More specifically, we define the unit of energy as  $\bar{E} \equiv \frac{\hbar^2}{mL^2} = \frac{2E_r}{\pi^2} \approx 4.466 \times 10^{-31}$  J.

In typical experiments, the optical lattice depth is varied in regimes of up to several tens of recoil energies (in

Quantity	MCTDH-X units
unit of length	$\bar{L} = \lambda_0/2 = 266.1 \text{ nm}$
opt. latt. sites	at -2, -1, 0, 1, 2
unit of energy	$\bar{E} = \frac{\hbar^2}{m\bar{L}^2} = \frac{2E_r}{\pi^2} \approx 4.466 \times 10^{-31} \text{ J}$
potential depth	$V = 400.0\bar{E} \approx 81 E_r$
on-site repulsion	$ g_0  = 400.0\bar{E} \approx 81 E_r$
dipolar interaction	e.g. $g_d = -1.0\bar{E} = -0.203 E_r$
unit of time	$\bar{t} \equiv \frac{m\bar{L}^2}{\hbar} = 59.03 \mu\text{s}$

TABLE I. Units used in MCTDH-X simulations.  $E_r = \frac{\hbar^2 k_0^2}{2m}$  is the recoil energy.

particular when lattice physics is quantum simulated). In our simulations, we probe similar regimes of  $V_0 = 40\bar{E} \approx 8E_r$  or  $V_0 = 100\bar{E} \approx 20E_r$ . The on-site interactions are kept at fixed magnitude  $|g_0| = 400\bar{E} \approx 81E_r$ , unless otherwise state. During the quench, we change only their sign (from repulsive to attractive). When we turn on dipolar interactions, we probe regimes up to strength  $|g_d| = 45\bar{E} \approx 9E_r$ , although in the main text we reported only results up to  $|g_d| = 10\bar{E} \approx 2E_r$  since the physics does not change qualitatively with stronger dipolar interactions.

### 3. Time

The unit of time is also defined from the unit of length, as  $\bar{t} \equiv \frac{m\bar{L}^2}{\hbar} = \frac{m\lambda_0^2}{\hbar} = 0.5903 \times 10^{-4} \text{ s} = 59.03 \mu\text{s}$ . In our simulations, we ran time evolutions up until around  $t \approx 10\bar{t} \approx 590.25 \text{ ms}$ . However, in thermalizing phases, the onset of thermalization is very rapid. Thus, we typically restrict our ranges to show only results up to  $t \approx 1\bar{t} \approx 59.03 \mu\text{s}$ .

#### Appendix C: Initial states

In this section we show the density profile for the initial states used in the quench protocol and studied in the main text. The initial states for the unit filling case can be seen in Fig. 12 while the ones for the double filling case are shown in Fig. 13. We remark that close to the transition between the Mott and cluster phases ( $g_d \approx 0.8E_r$ ) there is a strong competition between lattice localization, contact repulsion, and dipolar attraction. Furthermore, depending on the number of particles and sites used, frustration can emerge (for example 6 particles wanting to localize on two sites will not be pinned symmetrically around the central site in an optical lattice with an odd number of sites). As a consequence, the corresponding ground states can be quasidegenerate and spontaneously break the inversion symmetry of the lattice. This can lead to the states being pinned away from the central site of the optical lattice [see Fig. 12(c) and Fig. 13(b)].

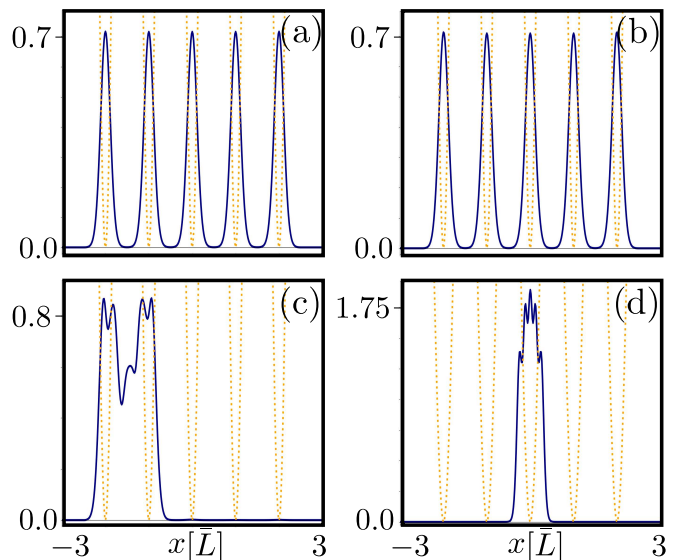


FIG. 12. Initial states (solid line) and optical lattice (dashed line, scaled down by 20 $\times$ ) used in the quench protocol for  $N = 5$  bosons and  $M = 10$  orbitals in  $S = 5$  sites (unit filling) with (a)  $g_d = 0.0E_r$ , (b)  $g_d = -0.57E_r$ , (c)  $g_d = -0.82E_r$ , (d)  $g_d = -2.02E_r$ . The other parameters are  $V_0 \approx 20E_r$  and  $|g_0| \approx 81E_r$ .

Nevertheless, we have verified that pinning at different sites does not lead to any qualitative differences in the density nor in the entropy dynamics.

#### Appendix D: Other measures of correlation

In this appendix we present the results for the one-body and two-body Glauber correlation functions  $g^{(1)}(x, x') = \frac{\rho^{(1)}(x, x')}{N\sqrt{\rho(x)\rho(x' )}}$  and  $g^{(2)}(x, x') = \frac{\rho^{(2)}(x, x')}{N^2\rho(x)\rho(x' )}$ . These quantities, shown in Figs. 14 to 17, provide a more comprehensive picture of the correlations in the system by normalizing the one-body density  $\rho^{(1)}(x, x')$  and two-body density  $\rho^{(2)}(x, x')$  with the particle number and density, although they conclude with the same physics drawn in the main text. We find that the dynamics of first-order and second-order coherence is strongly related to the many-body dynamical fragmentation. The parameters for post quench dynamics remain the same as described in the main text.

The results for the unit filling case are presented in Figs. 14 and 15. For the prequench state with  $g_d = 0.0E_r$  [Fig. 14(a)] and with  $g_d = -0.45E_r$  [Fig. 14(d)], the diagonal of the first order correlation function shows five completely separated coherent regions (bright lobes) where  $|g^{(1)}|^2 \approx 1$ . The coherence of bosons within the same well is maintained whereas the off-diagonal correlation ( $x \neq x'$ ) vanishes. This describes the five-fold fragmented fully localized Mott phase. The corresponding  $g^{(2)}$  in Figs. 15(a) and (d) shows five completely extinguished lobes (correlation holes), i.e. the probabil-



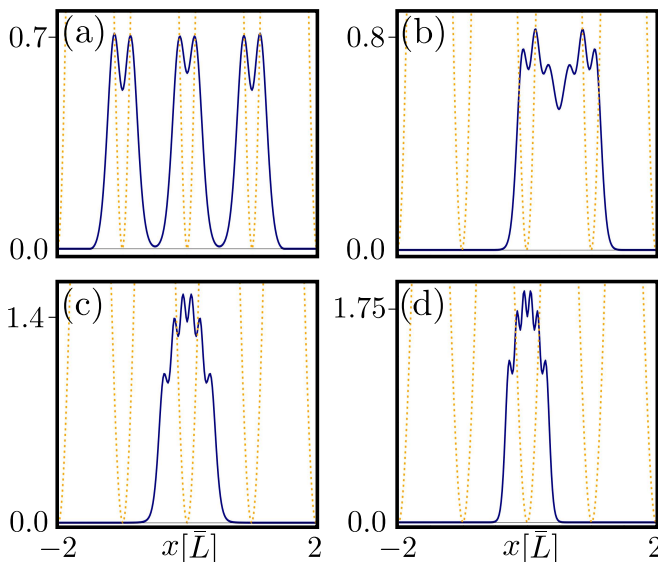


FIG. 13. Initial states (solid line) and optical lattice (dashed line, scaled down by  $20\times$ ) used in the quench protocol for  $N = 6$  bosons and  $M = 12$  orbitals in  $S = 3$  sites (double filling) with (a)  $g_d = 0.0E_r$ , (b)  $g_d = -0.82E_r$ , (c)  $g_d = -1.01E_r$ , (d)  $g_d = -2.02E_r$ . The other parameters are  $V_0 \approx 20E_r$  and  $|g_0| \approx 81E_r$ .

ity of finding two bosons in the same place ( $x = x'$ ) is zero. On the other hand, second order coherence is maintained between the wells. For  $g_d = 0.0E_r$ , as the many body state remains five-fold fragmented throughout the post quench dynamics, the corresponding correlation dynamics also remains stable as seen in Figs. 14(b)-(c) and 15(b)-(c). For  $g_d = -0.45E_r$ , the initially fully localized Mott state retains stability for long time but eventually becomes fully fragmented. This behavior is exemplified by the disappearance of diagonal correlation in one-body [Fig. 14(e)-(f)] and disruption of the correlation hole in two-body [Fig. 15(e)-(f)] coherence. However, the faded five spots across the diagonal exhibit the presence of five bosons before complete evaporation. For  $g_d = -0.82E_r$ , as the many-body state is clustered in two consecutive

lattice sites in one side, the corresponding one-body correlation is also confined with distinct many-body features [Fig. 14 (g)]. Upon quenching, coherence is gradually lost and finally evaporates as seen in Figs. 14 (h)-(i). The corresponding two-body coherence [Fig. 15 (g)] exhibits a correlation hole confined only to the two consecutive lattice in one side and in the post quench dynamics it follows the evaporation process (Figs. 15 (h)-(i)). For  $g_d = -2.02E_r$ , the one-body coherence is clustered in the central lattice [Fig. 14 (j)] and the correlation hole moves to the central position as well [Fig. 15 (j)]. During the post-quench dynamics, both one- and two-body coherence are lost with clear signature of many-body features.

In Figs. 16 and 17, we plot the one- and two-body correlation functions  $g^{(1)}$  and  $g^{(2)}$  for the double filling case where the fermionized Mott phase is perturbed by weak attractive long-range interaction. For the pre-quench state with  $g_d = 0.0E_r$  [Fig. 16(a)], the coherence between wells is already lost as  $|g^{(1)}|^2 \approx 0$  for all off-diagonal points ( $x \neq x'$ ). In addition, due to double occupation, the first order coherence within each well is designed by two distinct bright lobes signifying the presence of two fermionized bosons. The second order correlation function  $g^{(2)}$  has a fully developed correlation hole along the diagonal with distinct many-body features in each lattice site. During the post-quench dynamics, correlation in each well first expands and then is quickly lost [Figs. 16(b)-(c) and 17(b)-(c)]. For  $g_d = -0.82E_r$ , diagonal correlations are confined to two consecutive lattice sites [Fig. 16(d)]. Upon quenching, the structure of correlation is lost and only a thin thread-like diagonal correlation is retained before complete disruption (Fig 16(e)-(f)). Fig. 17(d) shows that the correlation hole stays along the diagonal of two consecutive lattice sites and then disappears with time (Fig. 17(e)-(f)) after the quench. Similarly, for  $g_d = -2.02E_r$ , as the atoms are centrally localized, both the diagonal one-body correlation and the correlation hole are confined in the central lattice site [Figs. 16(g) and 17(g)]. Upon quenching, correlation is lost maintaining a thin diagonal line showing the presence of bosons before total evaporation [Figs. 16(h)-(i) and 17(h)-(i)].

[1] J. Léonard, A. Morales, P. Zupancic, T. Esslinger, and T. Donner, Supersolid formation in a quantum gas breaking a continuous translational symmetry, *Nature* **543**, 87 (2017).  
 [2] J. Léonard, A. Morales, P. Zupancic, T. Donner, and T. Esslinger, Monitoring and manipulating higgs and goldstone modes in a supersolid quantum gas, *Science* **358**, 1415 (2017).  
 [3] J.-R. Li, J. Lee, W. Huang, S. Burchesky, B. Shteynas, F. Çağrı Top, A. O. Jamison, and W. Ketterle, A stripe phase with supersolid properties in spin-orbit-coupled bose-einstein condensates, *Nature* **543**, 91 (2017).

[4] F. Böttcher, J.-N. Schmidt, M. Wenzel, J. Hertkorn, M. Guo, T. Langen, and T. Pfau, Transient supersolid properties in an array of dipolar quantum droplets, *Phys. Rev. X* **9**, 011051 (2019).  
 [5] L. Tanzi, E. Lucioni, F. Famà, J. Catani, A. Fioretti, C. Gabbanini, R. N. Bisset, L. Santos, and G. Modugno, Observation of a dipolar quantum gas with metastable supersolid properties, *Phys. Rev. Lett.* **122**, 130405 (2019).  
 [6] L. Tanzi, S. M. Rocuzzo, E. Lucioni, F. Famà, A. Fioretti, C. Gabbanini, G. Modugno, A. Recati, and S. Stringari, Supersolid symmetry breaking from com-

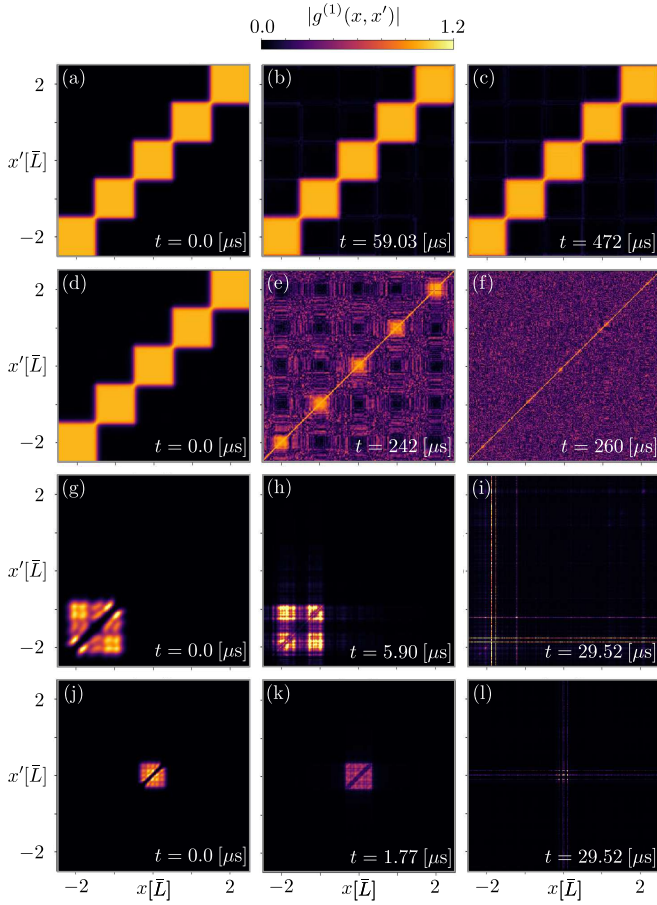


FIG. 14. Dynamics of the Glauber one-body correlation function  $g^{(1)}(x, x')$  post quench for  $N = 5$  bosons and  $M = 10$  orbitals with (a)-(c)  $g_d = 0.0E_r$ , (d)-(f)  $g_d = -0.45E_r$ , (g)-(i)  $g_d = -0.82E_r$ , (j)-(l)  $g_d = -2.02E_r$ . The other parameters are  $V_0 \approx 20E_r$  and  $|g_0| \approx 81E_r$ .

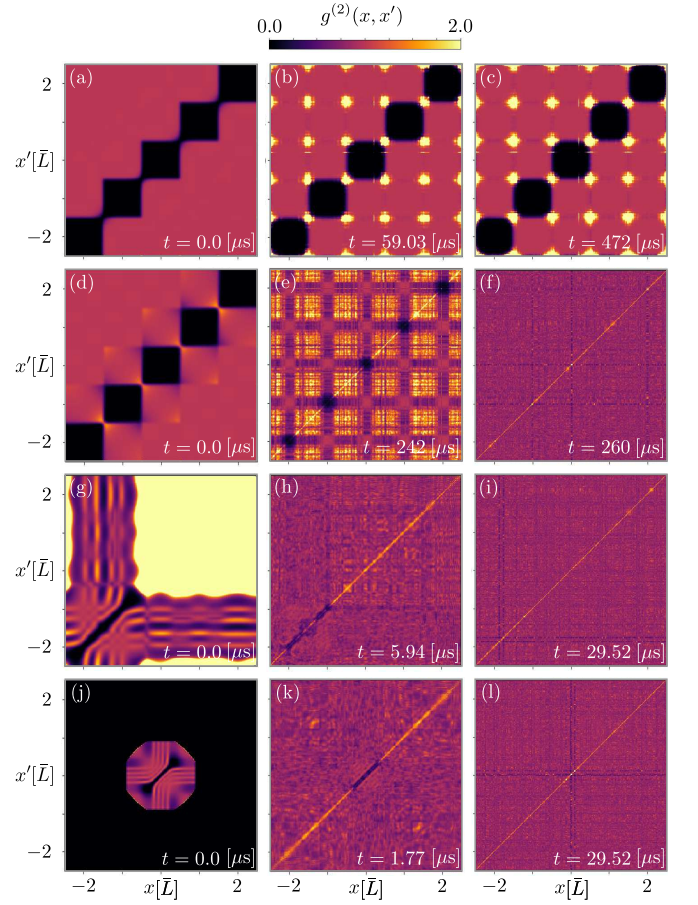


FIG. 15. Dynamics of the Glauber two-body correlation function  $g^{(2)}(x, x')$  post quench for  $N = 5$  bosons and  $M = 10$  orbitals with (a)-(c)  $g_d = 0.0E_r$ , (d)-(f)  $g_d = -0.45E_r$ , (g)-(i)  $g_d = -0.82E_r$ , (j)-(l)  $g_d = -2.02E_r$ . The other parameters are  $V_0 \approx 20E_r$  and  $|g_0| \approx 81E_r$ .

pressional oscillations in a dipolar quantum gas, *Nature* **574**, 382 (2019).

- [7] L. Chomaz, D. Petter, P. Ilzhöfer, G. Natale, A. Trautmann, C. Politi, G. Durastante, R. M. W. van Bijnen, A. Patscheider, M. Sohmen, M. J. Mark, and F. Ferlaino, Long-lived and transient supersolid behaviors in dipolar quantum gases, *Phys. Rev. X* **9**, 021012 (2019).
- [8] J. H. J.-N. S. M. W. H. P. B. T. L. . T. P. Mingyang Guo, Fabian Böttcher, The low-energy goldstone mode in a trapped dipolar supersolid, *Nature* **574**, 386 (2019).
- [9] G. Natale, R. M. W. van Bijnen, A. Patscheider, D. Petter, M. J. Mark, L. Chomaz, and F. Ferlaino, Excitation spectrum of a trapped dipolar supersolid and its experimental evidence, *Phys. Rev. Lett.* **123**, 050402 (2019).
- [10] L. Tanzi, J. G. Maloberti, G. Biagioni, A. Fioretti, C. Gabbanini, and G. Modugno, Evidence of superfluidity in a dipolar supersolid from nonclassical rotational inertia, *Science* **371**, 1162 (2021).
- [11] M. A. Norcia, C. Politi, L. Klaus, E. Poli, M. Sohmen, M. J. Mark, R. N. Bisset, L. Santos, and F. Ferlaino, Two-dimensional supersolidity in a dipolar quantum gas, *Nature* **596**, 357 (2021).
- [12] M. Sohmen, C. Politi, L. Klaus, L. Chomaz, M. J. Mark,

- M. A. Norcia, and F. Ferlaino, Birth, life, and death of a dipolar supersolid, *Phys. Rev. Lett.* **126**, 233401 (2021).
- [13] J. Sánchez-Baena, C. Politi, F. Maucher, F. Ferlaino, and T. Pohl, Heating a dipolar quantum fluid into a solid, *Nature Communications* **14**, 1868 (2023).
- [14] A. Recati and S. Stringari, Supersolidity in ultracold dipolar gases, *Nature Review Physics* **5**, 735 (2023).
- [15] J. Smits, L. Liao, H. T. C. Stoof, and P. van der Straten, Observation of a space-time crystal in a superfluid quantum gas, *Phys. Rev. Lett.* **121**, 185301 (2018).
- [16] H. Keßler, P. Kongkhambut, C. Georges, L. Mathey, J. G. Cosme, and A. Hemmerich, Observation of a dissipative time crystal, *Phys. Rev. Lett.* **127**, 043602 (2021).
- [17] P. Kongkhambut, J. Skulte, L. Mathey, J. G. Cosme, A. Hemmerich, and H. Keßler, Observation of a continuous time crystal, *Science* **377**, 670 (2022).
- [18] M. Aidelsburger, M. Lohse, C. Schweizer, M. Atala, J. T. Barreiro, S. Nascimbène, N. R. Cooper, I. Bloch, and N. Goldman, Measuring the chern number of hofstadter bands with ultracold bosonic atoms, *Nature Physics* **11**, 162 (2015).
- [19] C. Schweizer, F. Grusdt, M. Berngruber, L. Barbiero, E. Demler, N. Goldman, I. Bloch, and M. Aidelsburger,



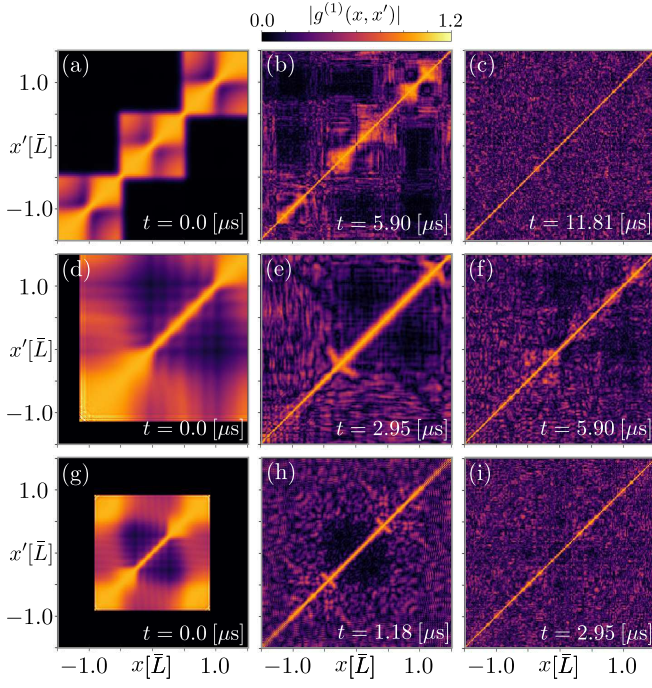


FIG. 16. Dynamics of the Glauber one-body correlation function  $g^{(1)}(x, x')$  post quench for  $N = 6$  bosons and  $M = 12$  orbitals in  $S = 3$  sites (double filling) with (a)-(c)  $g_d = 0.0E_r$ , (d)-(f)  $g_d = -0.82E_r$ , (g)-(i)  $g_d = -2.02E_r$ . The other parameters are  $V_0 \approx 20E_r$  and  $|g_0| \approx 81E_r$ .

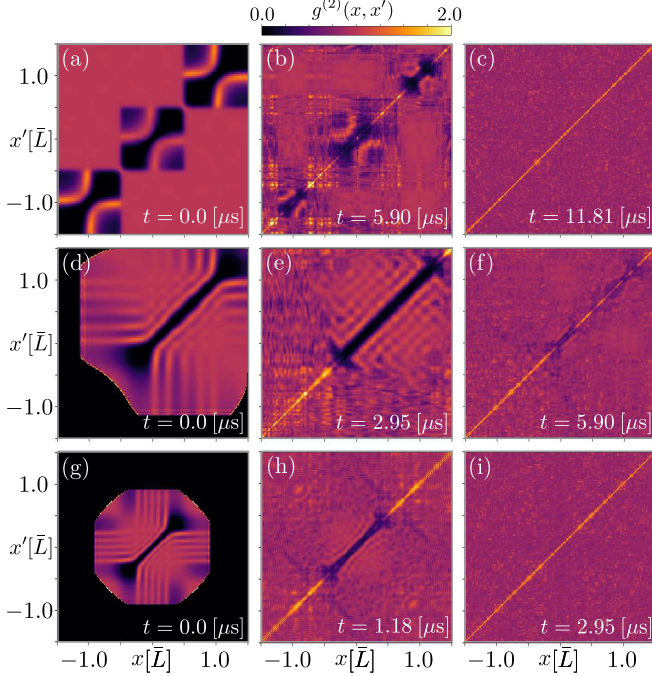


FIG. 17. Dynamics of the Glauber two-body correlation function  $g^{(2)}(x, x')$  post quench for  $N = 6$  bosons and  $M = 12$  orbitals in  $S = 3$  sites (double filling) with (a)-(c)  $g_d = 0.0E_r$ , (d)-(f)  $g_d = -0.82E_r$ , (g)-(i)  $g_d = -2.02E_r$ . The other parameters are  $V_0 \approx 20E_r$  and  $|g_0| \approx 81E_r$ .

Floquet approach to z2 lattice gauge theories with ultracold atoms in optical lattices, *Nature Physics* **15**, 1168 (2019).

- [20] J. Li, A. K. Harter, J. Liu, L. de Melo, Y. N. Joglekar, and L. Luo, Observation of parity-time symmetry breaking transitions in a dissipative floquet system of ultracold atoms, *Nature Communications* **10**, 855 (2019).
- [21] K. Wintersperger, C. Braun, F. N. Ünal, A. Eckardt, M. D. Liberto, N. Goldman, I. Bloch, and M. Aidelsburger, Realization of an anomalous floquet topological system with ultracold atoms, *Nature Physics* **16**, 1058 (2020).
- [22] C. A. Bracamontes, J. Maslek, and J. V. Porto, Realization of a floquet-engineered moat band for ultracold atoms, *Phys. Rev. Lett.* **128**, 213401 (2022).
- [23] B.-Y. Sun, N. Goldman, M. Aidelsburger, and M. Bukov, Engineering and probing non-abelian chiral spin liquids using periodically driven ultracold atoms, *PRX Quantum* **4**, 020329 (2023).
- [24] J.-Y. Zhang, C.-R. Yi, L. Zhang, R.-H. Jiao, K.-Y. Shi, H. Yuan, W. Zhang, X.-J. Liu, S. Chen, and J.-W. Pan, Tuning anomalous floquet topological bands with ultracold atoms, *Phys. Rev. Lett.* **130**, 043201 (2023).
- [25] G. E. Astrakharchik, J. Boronat, J. Casulleras, and S. Giorgini, Beyond the tonks-girardeau gas: Strongly correlated regime in quasi-one-dimensional bose gases, *Phys. Rev. Lett.* **95**, 190407 (2005).
- [26] M. T. Batchelor, M. Bortz, X. W. Guan, and N. Oelkers, Evidence for the super tonks-girardeau gas, *Journal of Statistical Mechanics: Theory and Experiment*, L10001 (2005).
- [27] E. Tempfli, S. Zöllner, and P. Schmelcher, Excitations of attractive 1d bosons: binding versus fermionization, *New Journal of Physics* **10**, 103021 (2008).
- [28] E. Haller, M. Gustavsson, M. J. Mark, J. G. Danzl, R. Hart, G. Pupillo, and H.-C. Nägerl, Realization of an excited, strongly correlated quantum gas phase, *Science* **325**, 1224 (2009).
- [29] W. Kao, K.-Y. Li, K.-Y. Lin, S. Gopalakrishnan, and B. L. Lev, Topological pumping of a 1d dipolar gas into strongly correlated prethermal states, *Science* **371**, 296 (2021).
- [30] L. Tonks, The complete equation of state of one, two and three-dimensional gases of hard elastic spheres, *Physical Review* **50**, 955 (1936).
- [31] M. D. Girardeau, Relationship between systems of impenetrable bosons and fermions in one dimension, *Journal of Mathematical Physics* **1**, 516 (1960).
- [32] M. D. Girardeau, Permutation symmetry of many-particle wave functions, *Phys. Rev.* **139**, B500 (1965).
- [33] M. Olshanii, Atomic scattering in the presence of an external confinement and a gas of impenetrable bosons, *Phys. Rev. Lett.* **81**, 938 (1998).
- [34] D. S. Petrov, G. V. Shlyapnikov, and J. T. M. Walraven, Regimes of quantum degeneracy in trapped 1d gases, *Phys. Rev. Lett.* **85**, 3745 (2000).
- [35] M. D. Girardeau, E. M. Wright, J. M. Triscari, K. Kheruntsyan, and I. Bouchoule, Ground-state properties of a one-dimensional system of hard-core bosons in a harmonic trap, *Physical Review A* **63**, 033601 (2001).
- [36] T. Kinoshita, T. Wenger, and D. S. Weiss, Observation of a one-dimensional tonks-girardeau gas, *Science* **305**, 1125 (2004).



- [37] B. Paredes, A. Widera, V. Murg, O. Mandel, S. Fölling, I. Cirac, G. V. Shlyapnikov, T. W. Hänsch, and I. Bloch, Tonks–girardeau gas of ultracold atoms in an optical lattice, *Nature* **429**, 277 (2004).
- [38] T. Jacqmin, J. Armijo, T. Berrada, K. V. Kheruntsyan, and I. Bouchoule, Sub-poissonian fluctuations in a 1d bose gas: from the quantum quasicondensate to the strongly interacting regime, *Physical Review Letters* **106**, 230405 (2011).
- [39] F. Mazzanti, G. E. Astrakharchik, J. Boronat, and J. Casulleras, Ground-state properties of a one-dimensional system of hard rods, *Phys. Rev. Lett.* **100**, 020401 (2008).
- [40] G. E. Astrakharchik and Y. E. Lozovik, Super-tonks-girardeau regime in trapped one-dimensional dipolar gases, *Phys. Rev. A* **77**, 013404 (2008).
- [41] L. Guan and S. Chen, Super-tonks-girardeau gas of spin 1/2 interacting fermions ground-state properties of a one-dimensional system of hard rods, *Phys. Rev. Lett.* **105**, 175301 (2010).
- [42] S. Murmann, F. Deuretzbacher, G. Zürn, J. Bjerlin, S. Reimann, L. Santos, T. Lompe, and S. Jochim, Antiferromagnetic heisenberg spin chain of a few cold atoms in a one-dimensional trap, *Phys. Rev. Lett.* **115**, 215301 (2015).
- [43] Y. Chen and X. Cui, Ultrastable super-tonks-girardeau gases under weak dipolar interactions, *Phys. Rev. Lett.* **131**, 203002 (2023).
- [44] I. Morera, R. Oldziejewski, G. E. Astrakharchik, and B. Julia-Diaz, Superexchange liquefaction of strongly correlated lattice dipolar bosons, *Phys. Rev. Lett.* **130**, 023602 (2023).
- [45] M. Marciniak, M. Lebek, J. Kopycinski, W. Gorecki, R. Oldziejewski, and K. Pawłowski, Super-tonks-girardeau quench in the extended bose-hubbard model, *Phys. Rev. A* **108**, 043304 (2023).
- [46] A. I. Streltsov, O. E. Alon, and L. S. Cederbaum, General variational many-body theory with complete self-consistency for trapped bosonic systems, *Phys. Rev. A* **73**, 063626 (2006).
- [47] A. I. Streltsov, O. E. Alon, and L. S. Cederbaum, Role of excited states in the splitting of a trapped interacting bose-einstein condensate by a time-dependent barrier, *Phys. Rev. Lett.* **99**, 030402 (2007).
- [48] O. E. Alon, A. I. Streltsov, and L. S. Cederbaum, Unified view on multiconfigurational time propagation for systems consisting of identical particles, *J. Chem. Phys.* **127**, 154103 (2007).
- [49] O. E. Alon, A. I. Streltsov, and L. S. Cederbaum, Multiconfigurational time-dependent hartree method for bosons: Many-body dynamics of bosonic systems, *Phys. Rev. A* **77**, 033613 (2008).
- [50] A. U. J. Lode, Multiconfigurational time-dependent hartree method for bosons with internal degrees of freedom: Theory and composite fragmentation of multi-component bose-einstein condensates, *Phys. Rev. A* **93**, 063601 (2016).
- [51] E. Fasshauer and A. U. J. Lode, Multiconfigurational time-dependent hartree method for fermions: Implementation, exactness, and few-fermion tunneling to open space, *Phys. Rev. A* **93**, 033635 (2016).
- [52] A. U. J. Lode, C. Lévêque, L. B. Madsen, A. I. Streltsov, and O. E. Alon, Colloquium: Multiconfigurational time-dependent hartree approaches for indistinguishable particles, *Rev. Mod. Phys.* **92**, 011001 (2020).
- [53] R. Lin, P. Molignini, L. Papariello, M. C. Tsatsos, C. Lévêque, S. E. Weiner, E. Fasshauer, and R. Chitra, Mctdh-x: The multiconfigurational time-dependent hartree method for indistinguishable particles software, *Quantum Sci. Technol.* **5**, 024004 (2020).
- [54] A. U. J. Lode, M. C. Tsatsos, E. Fasshauer, S. E. Weiner, R. Lin, L. Papariello, P. Molignini, C. Lévêque, M. Büttner, J. Xiang, S. Dutta, and Y. Bilinskaya, Mctdh-x: The multiconfigurational time-dependent hartree method for indistinguishable particles software (2024).
- [55] C. Neill, P. Roushan, M. Fang, Y. Chen, M. Kolodrubetz, Z. Chen, A. Megrant, R. Barends, B. Campbell, B. Chiaro, A. Dunsworth, E. Jeffrey, J. Kelly, J. Mutus, P. J. J. O’Malley, C. Quintana, D. Sank, A. Vainsencher, J. Wenner, T. C. White, A. Polkovnikov, and J. M. Martinis, Ergodic dynamics and thermalization in an isolated quantum system., *Nature Phys* **12**, 1037 (2016).
- [56] M. Gring, M. Kuhnert, T. Langen, T. Kitagawa, B. Rauer, M. Schreitl, I. Mazets, D. A. Smith, E. Demler, and J. Schmiedmayer, Relaxation and prethermalization in an isolated quantum system, *Science* **337**, 1318 (2012).
- [57] T. Langen, S. Erne, R. Geiger, B. Rauer, T. Schweigler, M. Kuhnert, W. Rohringer, I. E. Mazets, T. Gasenzer, and J. Schmiedmayer, Experimental observation of a generalized gibbs ensemble, *Science* **348**, 207 (2015).
- [58] T. G. Tim Langen and J. Schmiedmayer, Prethermalization and universal dynamics in near-integrable quantum systems, *Journal of Statistical Mechanics: Theory and Experiment* , 064009 (2016).
- [59] Y. Tang, W. Kao, K.-Y. Li, S. Seo, K. Mallayya, M. Rigol, S. Gopalakrishnan, and B. L. Lev, Thermalization near integrability in a dipolar quantum newton’s cradle, *Phys. Rev. X* **8**, 021030 (2018).
- [60] K. Mallayya, M. Rigol, and W. D. Roeck, Prethermalization and thermalization in isolated quantum systems, *Phys. Rev. X* **9**, 021027 (2019).
- [61] E. Tiesinga, C. J. Williams, F. H. Mies, and P. S. Julienne, Interacting atoms under strong quantum confinement, *Phys. Rev. A* **61**, 063416 (2000).
- [62] T. Bergeman, M. G. Moore, and M. Olshanii, Atom-atom scattering under cylindrical harmonic confinement: Numerical and analytic studies of the confinement induced resonance, *Phys. Rev. Lett.* **91**, 163201 (2003).
- [63] J. I. Kim, J. Schmiedmayer, and P. Schmelcher, Quantum scattering in quasi-one-dimensional cylindrical confinement, *Phys. Rev. A* **72**, 042711 (2005).
- [64] V. A. Yurovsky, Feshbach resonance scattering under cylindrical harmonic confinement, *Phys. Rev. A* **71**, 012709 (2005).
- [65] V. S. Melezhik, J. Kim, and P. Schmelcher, Wave-packet dynamical analysis of ultracold scattering in cylindrical waveguides, *Phys. Rev. A* **76**, 053611 (2007).
- [66] S. Saeidian, V. Melezhik, and P. Schmelcher, Multi-channel atomic scattering and confinement-induced resonances in waveguides, *Phys. Rev. A* **77**, 042721 (2008).
- [67] G.P.Berman, F. Borgonovi, and F. M. Izrailev, Irregular dynamics in a one-dimensional bose system, *Phys. Rev. Lett.* **92**, 030404 (2004).
- [68] A. U. J. Lode, B. Chakrabarti, and V. K. B. Kota, Many-body entropies, correlations, and emergence of statistical relaxation in interaction quench dynamics of ultracold bosons, *Phys. Rev. A* **92**, 033622 (2015).
- [69] M. Rigol, V. Dunjko, V. Yurovsky, and M. Olshanii, Re-

- laxation in a completely integrable many-body quantum system: An ab initio study of the dynamics of the highly excited states of 1d lattice hard-core bosons, *Phys. Rev. Lett.* **98**, 050405 (2007).
- [70] Z. X. Gong and L. M. Duan, Prethermalization and dynamic phase transition in an isolated trapped ion spin chain, *New J. Phys.* **15**, 113051 (2013).
- [71] V. K. B. Kota and R. Sahu, Single-particle entropy in (1+2)-body random matrix ensembles, *Phys. Rev. E* **66**, 037103 (2002).
- [72] L. Chomaz, I. Ferrier-Barbut, F. Ferlaino, B. Laburthe-Tolra, B. L. Lev, and T. Pfau, Dipolar physics: a review of experiments with magnetic quantum gases, *Rep. Prog. Phys.* **86**, 026401 (2023).
- [73] P. Mognini, C. L ev eque, H. Ke bler, D. Jaksch, R. Chitra, and A. U. J. Lode, Crystallization via cavity-assisted infinite-range interactions, *Phys. Rev. A* **106**, L011701 (2022).
- [74] L. Novotny, J. Vijayan1, J. Piotrowski, C. Gonzalez-Ballester, K. Weber, and O. Romero-Isart, Cavity-mediated long-range interactions in levitated optomechanics, (2023).
- [75] P. Mognini, L. Papariello, A. U. J. Lode, and R. Chitra, Superlattice switching from parametric instabilities in a driven-dissipative bose-einstein condensate in a cavity, *Phys. Rev. A* **98**, 053620 (2018).
- [76] R. Lin, L. Papariello, P. Mognini, R. Chitra, and A. U. J. Lode, Superfluid–mott-insulator transition of ultracold superradiant bosons in a cavity, *Phys. Rev. A* **100**, 013611 (2019).
- [77] R. Lin, P. Mognini, A. U. J. Lode, and R. Chitra, Pathway to chaos through hierarchical superfluidity in blue-detuned cavity-bec systems, *Phys. Rev. A* **101**, 061602(R) (2020).
- [78] R. Lin, C. Georges, J. Klinder, P. Mognini, M. B uttner, A. U. J. Lode, R. Chitra, A. Hemmerich, and H. Kessler, Mott transition in a cavity-boson system: A quantitative comparison between theory and experiment, *SciPost Phys.* **11**, 030 (2021).
- [79] M. Hughes, A. U. J. Lode, D. Jaksch, and P. Mognini, Accuracy of quantum simulators with ultracold dipolar molecules: A quantitative comparison between continuum and lattice descriptions, *Phys. Rev. A* **107**, 033323 (2023).
- [80] S. Moudgalya, B. A. Bernevig, and N. Regnault, Quantum many-body scars and hilbert space fragmentation: a review of exact results, *Rep. Prog. Phys.* **85**, 086501 (2022).
- [81] N. Yonezawa, A. Tanaka, and T. Cheon, Quantum holonomy in the lieb-liniger model, *Phys. Rev. A* **87**, 062113 (2013).
- [82] K. Sim, R. Chitra, and P. Mognini, Quench dynamics and scaling laws in topological nodal loop semimetals, *Phys. Rev. B* **106**, 224302 (2022).
- [83] K. Sim, N. Defenu, P. Mognini, and R. Chitra, Quantum metric unveils defect freezing in non-hermitian systems, *Phys. Rev. Lett.* **131**, 156501 (2023).
- [84] P. Kramer and M. Saraceno, *Geometry of the Time-Dependent Variational Principle in Quantum Mechanics*, Lecture Notes in Physics, Vol. 140 (Springer, 1981).
- [85] S. Kvaal, Variational formulations of the coupled-cluster method in quantum chemistry, *Molecular Physics* **111**, 1100 (2013).
- [86] A. McLachlan, A variational solution of the time-dependent schrodinger equation, *Molecular Physics* **8**, 39 (1964).
- [87] L. Cao, V. Bolsinger, S. I. Mistakidis, G. M. Koutentakis, S. Kr onke, J. M. Schurer, and P. Schmelcher, A unified ab initio approach to the correlated quantum dynamics of ultracold fermionic and bosonic mixtures, *J. Chem. Phys.* **147**, 044106 (2017).
- [88] S. H. J. S. A. Griesmaier, J. Werner and T. Pfau, Bose-einstein condensation of chromium, *Phys. Rev. Lett.* **94**, 160401 (2005).
- [89] T. Lahaye, J. Metz, B. Fr ohlich, T. Koch, M. Meister, A. Griesmaier, T. Pfau, H. Saito, Y. Kawaguchi, and M. Ueda, d-wave collapse and explosion of a dipolar bose-einstein condensate, *Phys. Rev. Lett.* **101**, 080401 (2008).